



Contents lists available at ScienceDirect

Journal of Applied Geophysics

journal homepage: www.elsevier.com/locate/jappgeo

Q1 Water prospection in volcanic islands by Time Domain Electromagnetic (TDEM) surveying: The case study of the islands of Fogo and Santo Antão in Cape Verde

Q2 F.J. Martínez-Moreno*, F.A. Monteiro-Santos, J. Madeira, I. Bernardo, A. Soares, M. Esteves, F. Adão

Instituto Dom Luiz, Universidade de Lisboa, Faculdade de Ciências, Campo Grande, Edif. C8, Lisboa, Portugal

ARTICLE INFO

Article history:

Received 13 May 2016

Received in revised form 22 August 2016

Accepted 15 September 2016

Available online xxxxx

Keywords:

Time Domain Electromagnetics (TDEM)

Cape Verde

Volcanic islands

Groundwater resources

Trade winds

ABSTRACT

Water demand in islands, focused in agriculture, domestic use and tourism, is usually supplied by groundwater. Thus the information about groundwater distribution is an important issue in islands water resources management. Time Domain Electromagnetic (TDEM) provides underground resistivity distribution at greater depths and is of easier application than other methods. In this study TDEM technique was used for groundwater prospection in two volcanic islands with water supply problems, the islands of Fogo and Santo Antão in the Republic of Cape Verde. The 10 islands of Cape Verde Archipelago, located off the coast of Senegal (W Africa), present a semi-arid climate and thus suffer from irregular and scarce precipitation. In the Island of Fogo 26 TDEM soundings, presenting an area distribution, were performed on the SW flank of the volcanic edifice. These allowed obtaining a 3D model composed of 5 layers parallel to the topographic surface separated by 50 m depth down to – 250 m. The results indicate the presence of the water-table at a depth of 150 m in the lower ranges of the W flank of the island, and at >200 m depth in the area above 250 m above sea level (a.s.l.). In the Island of Santo Antão 32 TDEM soundings, distributed along 5 linear profiles, were obtained on the north-eastern half of the island. The profiles are located in two regions exposed to different humidity conditions to the N and S of the main water divide. The northern flank receives the dominant trade winds first and most of the precipitation and, therefore, the water-table is shallower (~50 m depth) than in the S (~100 m depth). Our study demonstrates the applicability and usefulness of the TDEM method for groundwater prospection in high resistivity contexts such as in volcanic islands.

© 2016 Published by Elsevier B.V.

1. Introduction

Volcanic ocean islands represent isolated hydrogeological systems. The hydrogeological characteristics of each island are dependent on climate conditions (that determine precipitation regimes, vegetation cover and soil development), topography, geology (including lithology, structure and rock permeability), land use and water resources exploitation (Healy, 2010). The most relevant geological structures present in volcanic islands from a hydrogeological standpoint are: (i) the presence of an island basement usually presenting low permeability; (ii) the geometry of dike swarms that control the aquifers behaviour; (iii) the occurrence of impermeable layers (i.e. paleosols, sediments or compacted ash deposits) interbedded in the lava sequences supporting perched aquifers; and (iv) weathered landslide breccias at the base of large flank collapse surfaces acting as impermeable layers (Martí et al., 1997; Santamarta Cerezal, 2013; Marques et al., 2014).

Aquifer recharge in islands may occur in two different ways: by direct rainfall and by fog precipitation. The direct rainfall is conditioned by the

island geographical location, altitude and morphology. The second type of aquifer recharge in islands is produced by condensation of clouds, formed by adiabatic cooling of trade winds forced upwards, which may represent 1.5 to 3 times the amount of rainfall (Santamarta Cerezal and Seijas Bayón, 2010; Figueira et al., 2013). This kind of winds transports a high amount of water that is captured by the forest or is directly discharged when it finds topographic barriers (Johnson et al., 2014).

In volcanic islands, the proportion between runoff, evapotranspiration and groundwater recharge is determined by surface permeability, soil water storage, topographic slope, bare-soil evaporation and plant transpiration (Flint et al., 2013). Usually, volcanic islands do not have runoff water in the form of permanent rivers. This is due to incipient soil development at high elevations in addition to significant fracturing of rock outcrops, which favours water infiltration. Thus, most infiltration and groundwater recharge occurs in the higher reaches of the islands resulting from the combination of higher precipitation, greater permeability induced by fractures, and the frequent occurrence of closed basins (craters, calderas, and other closed depressions of various types) (Heilweil et al., 2008).

Dike intrusions are a distinctive feature in volcanic islands hydrogeology because they act as water flow barriers within the geologic structure

* Corresponding author.

E-mail address: fjmoreno@fc.ul.pt (F.J. Martínez-Moreno).

generating isolated aquifers at different water-table altitudes. These volcanic structures typically present near-vertical dips and thicknesses less than 3 m. Dikes behave as impermeable walls that divide the island underground into separated compartments from a hydrogeological point of view (MacDonald et al., 1983). Each of them represents local aquifers ranging from low altitude – low gradient regional water-tables located near sea level (areas usually characterized by low topographic slope), to high altitude – high gradient water-tables in topographically higher regions (usually more rugged morphologies) (Liu et al., 1983; Jackson and Lenat, 1989; Gingerich and Oki, 2000).

Water demand in islands is mostly due to agriculture activity and to domestic use. Water consumption by touristic demand, which requires increased amounts of water, may also play a significant role depending on the archipelago (López-Guzmán et al., 2015). In the islands most of the water used in human activities is groundwater since surface water is commonly scarce or even absent (Custodio, 1978). For this reason, the information on groundwater distribution is an important issue in island water resources management. In areas where wells, boreholes and drills are abundant, hydrogeological studies can be performed directly. In the absence of wells or when the spacing between them is large, the hydrogeological information they may provide is insufficient and non-representative. In this context, the search for groundwater resources must be addressed by geophysical prospecting.

Time Domain Electromagnetic (TDEM) – or *transient* – is a reliable geophysical technique to determine groundwater distribution in a specific area. TDEM method provides underground resistivity distribution so that the presence of the fresh water-table or saltwater produces a sudden change in resistivity from high resistivity values (in unsaturated rocks) to low or very low ones (in saturated rocks). This technique has

been employed in various specific geological contexts for groundwater prospecting (Goldman et al., 1994; Sananikone, 1998; Descloitres et al., 2000; Yechieli et al., 2001; Hoareau et al., 2007; Descloitres et al., 2013; Ruiz-Constán et al., 2015).

This study was primarily motivated by the need to obtain information about groundwater distribution in areas with water supply problems in the islands of Fogo and Santo Antão in the Cape Verde archipelago (Central Atlantic Ocean). Thus, the aim of this work is mainly focused in determining groundwater distribution using TDEM data in these two islands. With this purpose a network of TDEM station was installed in areas with no previous geophysical data.

2. Geological framework

The ten major islands forming the Cape Verde Archipelago (República de Cabo Verde, Fig. 1a) display a horseshoe shape open to the west. The archipelago is located 600 km to the W of the coast of Senegal (W Africa). The islands are traditionally divided into two groups related to the dominant Trade Winds: the Barlavento (windward) Group comprising the islands of Santo Antão, São Vicente, Santa Luzia, São Nicolau, Sal, and Boavista, and the Sotavento (leeward) Group that includes the islands of Brava, Fogo, Santiago and Maio. The archipelago was built on Late Jurassic to Cretaceous oceanic crust on top of a major topographic anomaly – the Cape Verde Rise. The magmatism is considered to be the result of a mantle plume (White, 1989) and the ages of the oldest subaerial lavas suggest that the islands emerged during the Miocene (Mitchell et al., 1983; Torres et al., 2002; Plesner et al., 2003; Duprat et al., 2007; Holm et al., 2008; Madeira et al., 2010; Dyhr and Holm, 2010; Ramalho et al., 2010; Ancochea et al., 2010; Ancochea

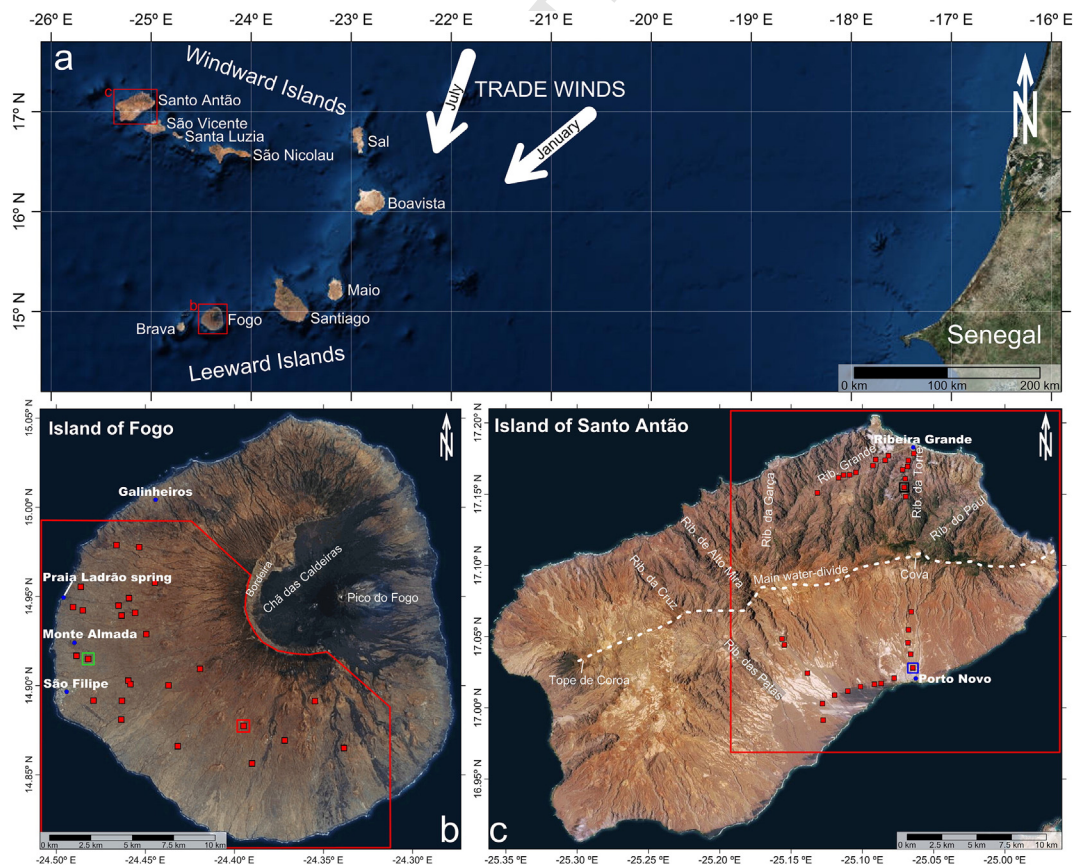


Fig. 1. Geographical location of the Cape Verde archipelago and the studied islands (a). The location of TDEM soundings (red squares) is shown on orthophoto images of the study areas of Fogo (a) and Santo Antão (b). The study area of each island is indicated by a red line. The red, green, blue and brown squares identify the TDEM stations displayed in Fig. 3. (For interpretation of the references to colour in this figure legend, the reader is referred to the web version of this article.)

et al., 2014; Ancochea et al., 2015). The morphology of the islands is related to their age, with the younger islands presenting vigorous morphologies that contrast with the razed topography of easternmost older islands of Sal, Boavista and Maio.

The islands of Santo Antão and Fogo, two of the youngest, are located on the western tips of the two arms of the U-shaped archipelago. Fogo is the fourth largest island with a surface area of 476 km², culminating at 2829 m above sea level (a.s.l.) at Pico do Fogo which represents the highest elevation in the archipelago. The island is formed by a major conical and slightly asymmetrical Quaternary strato-volcano. It is mostly formed by basanitic lava flow piles with minor intercalations of pyroclastic and sedimentary layers (Fig. 2a). A small outcrop of an older (Pliocene) basement formed by intrusive carbonatites (Hoernle et al., 2002) covered by lavas from the Intermediate and Younger volcanic units lies 3 km to the N of the city of São Filipe. The summit of the volcano is truncated by an 8 km-wide depression (Chã das Caldeiras; Fig. 1b) open to the E and surrounded on the other sides by an almost vertical wall (Bordeira). Rising from the flat floor of the depression is the young cone of Pico do Fogo. The depression is interpreted as the result of a major collapse of the E flank of the volcanic edifice (Day et al., 1999) or a combination of two caldera collapses followed by the failure of the E flank (Brum da Silveira et al., 1997; Madeira et al., 2008; Ramalho et al., 2015). The outer slopes are covered by pre-historical post-collapse lava flows issued from parasitic cones, aligned on radial and concentric feeder dikes, extending from the caldera rim to sea level. The NE flank is displaced by a graben structure bound by NE-SW fault scarps, the most conspicuous of which is the Galinheiros Fault. The caldera and the flank collapse scar are floored by historical lava flows and locally by lahars (Ribeiro, 1960; Torres et al., 1998). The latest Fogo eruption occurred on November 23rd, 2014 and lasted until early February 2015.

The island presents a constructive volcanic morphology that is perturbed by the caldera and flank collapse depressions. The drainage pattern is radial in the outer flanks of the main volcano. Inside the depression there is no developed drainage except for the E flank of Pico

do Fogo where several streams are incised on the pyroclasts and lahar deposits. The morphological asymmetry is, like in Santo Antão, the result of the dominant north-easterly trade winds. Most precipitation falls on the windward flank and thus the slopes are steeper and the streams more incised. The N littoral is also characterized by taller sea cliffs.

Santo Antão is the second largest island in Cape Verde with a surface area of 779 km² and rising to 1980 m a.s.l. at Tope de Coroa volcano, the second highest elevation in the archipelago. Geologically the island corresponds to an elongated NE-SW trending shield volcano that was fed by fissure volcanism along a dense dike swarm (Fig. 2b). The dike swarm follows the axial regions of the island and is well exposed in the deepest valleys of Ribeira das Patas, Ribeira da Garça and Ribeira Grande (Fig. 1c). The orientation of the later valley is certainly controlled by the dike structure since it is perpendicular to the slope of the N flank. The dominant direction of the dikes is NE-SW and its density decreases towards the coastal areas. These dikes fed the different building phases of the volcanic edifice. The most voluminous volcanism, corresponding to the main shield building phase (Older and Intermediate Volcanics, Holm et al., 2006), is represented by a thick pile of dominantly basanitic lava flows; in the northeast tip the sequence culminates with pyroclastic flow deposits related to hydromagmatic eruptions to the S and northeast of Cova crater. This volcanic building was later covered by smaller volume volcanic phases (Younger Volcanics, Holm et al., 2006). Besides basanitic lava flows, the younger volcanic phases produced abundant explosive deposits of more evolved compositions (phonolite) represented by plinian pumice fall, ignimbrite and block and ash flow deposits (Eisele et al., 2015).

The morphology of Santo Antão reflects its volcanic structure and is mostly a constructive surface corresponding to a narrow plateau punctuated by monogenetic cones and craters that descends towards the sea by relatively steep slopes. This volcanic morphology is dissected by some deeply incised fluvial basins (i.e. Ribeira das Patas, in the S slope and Ribeiras do Paul, da Torre, Grande, de Alto Mira, da Garça and da Cruz on the N; Fig. 1c), while most other streams present a relatively

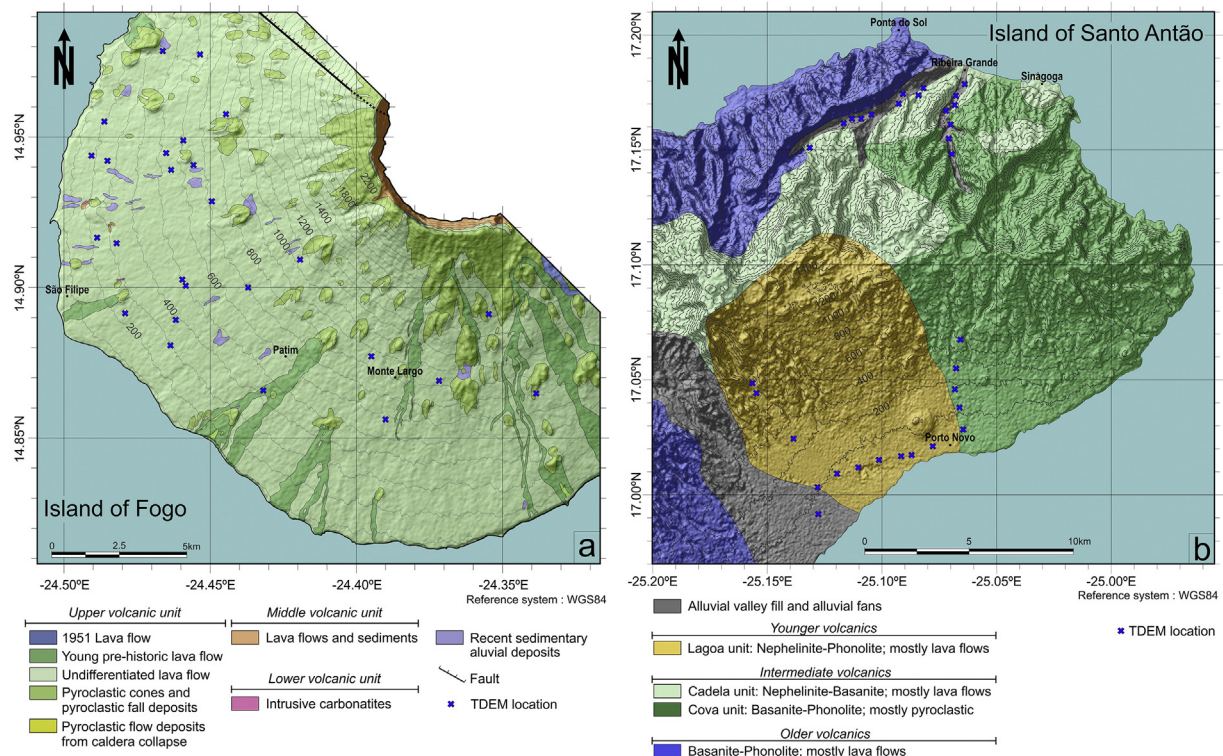


Fig. 2. Simplified geologic maps of the study areas in Fogo (a) and Santo Antão (b). The blue crosses indicate the TDEM soundings location. Geological sketch of Santo Antão modified from Holm et al. (2006). (For interpretation of the references to colour in this figure legend, the reader is referred to the web version of this article.)

incipient degree of incision. There is a marked contrast of the fluvial incision from the deeply carved N and S flanks as a result of the dominant NE-blowing trade winds. After crossing the ridge of the island, the wind is almost devoid of humidity so the rain is scarce and the landscape is arid in the S flank. The shore line presents the same contrast with taller cliffs due to the stronger wave erosion on the N coast when compared to the leeward littoral.

3. Method and survey setting

Time Domain Electromagnetic is based on the induction of a current waveform through a cable forming a loop on the surface followed by rapid current shut-offs. After each current shut-off, the disturbance through the transmitter loop generates a primary magnetic field that is in phase with the transmitter current. Later, a secondary magnetic field is created and its decay is measured by the receiver coil (Nabighian, 1988; Ward et al., 1990; Everett, 2013).

The apparent resistivity (ρ_a) is calculated through the mutual impedance $Z(t)$ at time (t) as (see, e.g. Bortolozzo et al., 2015):

$$\rho_a(t) = \left[\frac{\sqrt{\pi} a^2 n b^2}{20Z(t)} \right]^{\frac{2}{3}} \left(\frac{\mu_0}{t} \right)^{\frac{5}{3}} \quad (1)$$

where a is the current loop radius and b the receiver loop radius, n represents the number of turns, and μ_0 the free space magnetic permeability. The apparent resistivity values for each sounding were inverted using an iterative approach based on the Levenberg-Marquardt method and Singular Value Decomposition (SVD) technique. This procedure can be seen as an optimization one where an initial model is modified until an expected misfit between data and model response is reached. The modification of the model (Δm) at iteration k is calculated by,

$$\left(J(m^k)^T J(m^k) + \lambda I \right) \Delta m = -J(m^k)^T F(m^k) \quad (2)$$

where J is the Jacobian matrix, F represents the difference between data and model response in the logarithmic domain, λ is the damping factor and I the identity matrix. The system of equation is solved using the SVD technique.

The TDEM method was applied to detect the water-table depth and geometry in Fogo and Santo Antão islands. The high resistivity contrast between dry host rock and the saturated level allows determining the water-table depth below each measurement station. TDEM data was measured using the TEM-Fast48 equipment from Applied Electromagnetic Research (AEMR Inc.; Fainberg, 1999). This technique can be used in different configurations depending on the objectives to be achieved (Nicaise et al., 2013). The measurements were acquired in a single square loop configuration combining transmitter and receiver functions, with 50×50 m or 100×100 m loops depending on the terrain features. The data was processed with TEM-RES v.7.0 software from AEMR, which allows 1D modelling and inversion of the TDEM data. When necessary, the noisy data was firstly removed. The theoretical curve was fitted to the observed data applying trial-error methods and automatic inversion (Fig. 3). The fitting between modelled curves (lines in Fig. 3a, c) and data (points in the same fig.) was evaluated by direct observation since the program does not provide a quantitative assessment. The criterion in the selection of the final model is based on the minimum number of layers for the same quality of fitting.

In both islands the distribution of TDEM soundings is heterogeneous because of the rough topography and limited road access. In Fogo 26 soundings were performed on the southwest flank of the island covering an area of around 270 km^2 (Figs. 1b, 2a). The stations are as homogeneously distributed in the study area as possible, with spacing varying from 400 to 3500 m. In most soundings the loop dimension was 100×100 m with the applied current of 1 A (ampere). The soundings allowed depths of investigation of ~ 250 m on average providing a

geolectrical signature of the upper aquifer. A 3D view was obtained after 1D inversion of the data producing layers at each 50 m in depth, from 50 to 250 m below the surface. These layers were obtained extracting the resistivity values at each depth from the 1D inversion results and applying the kriging method with linear interpolation.

In Santo Antão 32 TDEM soundings were measured along 5 profiles on the north-eastern half of the island (Fig. 1c, 2b). The profiles on the northern slope were obtained along the valley bottoms of Ribeira Grande (P1) and Ribeira da Torre (P2) rivers. The remaining three profiles, on the southern flank of the island, followed the main roads of the area. Most soundings were performed using loops of 50×50 m with a transmitted current of 4 A. The investigation depth exceeded 100 m which allowed detecting the upper surface of the aquifers or deeper. 2D resistivity sections were created along the profiles using the sections mode of the TEM-RES program.

4. TDEM results

4.1. Island of Fogo

Most TDEM soundings were located at elevations between 250 and 750 m a.s.l. with the exception of 5 of them that are located higher and at maximum elevations of 1250 m a.s.l. (Fig. 2). No transient soundings were performed on coastal areas or inside the volcanically active caldera where most of the historical eruptions occurred.

The 3D view of the final models (Fig. 4) – composed of slices separated by 50 m in depth – shows that the 2 uppermost layers (at 50 and 100 m depths) detect high resistivities in excess of $1000 \Omega \cdot \text{m}$ (ohms \times metre) in the higher elevations and resistivities between 500 and $1000 \Omega \cdot \text{m}$ in the lower topographic areas. There is a small area in the SW side of the island, near the coast line, that presents resistivities of about $200 \Omega \cdot \text{m}$.

At the depth of 150 m lower resistivity values of $\sim 15 \Omega \cdot \text{m}$ were obtained in a region located on the WSW side of the island, which extends towards the S. This southward extension of the very low resistivities is more evident at the depth of 200 m, while at this depth the resistivity for the higher elevation areas decreases below $1000 \Omega \cdot \text{m}$. Finally, at 250 m depth most areas between 250 and 1000 m a.s.l. present resistivity values below $10 \Omega \cdot \text{m}$.

It is important to mention that the coastal areas located on the SW side – mainly in the layer of 150 m depth – present resistivities lower than the adjacent ones due to the absence of TDEM sounding and to kriging interpolation effects (see marked area in Fig. 4). Thus, the model must be interpreted with caution in this area.

4.2. Santo Antão Island

Five profiles were inverted on the N (along the valleys of Ribeira Grande – P1 and Ribeira da Torre – P2) and S (along the main roads – P3 to P5) flanks of northeast Santo Antão (Fig. 5). The northern profiles have NW-SE (P1) and NNW-SSE (P2) orientations. All the TDEM soundings located at the N are located along the bottom of river valleys at low elevations (from 40 to 170 m a.s.l.). Profile 1 is 7 km long and displays 3 layers separated by marked contrast in resistivity values. The shallower layer, with resistivities ranging from ~ 50 to $\sim 100 \Omega \cdot \text{m}$, has an average thickness of 50 m at higher elevations and ~ 20 m at lower altitudes. Below this layer the resistivity decreases to $5\text{--}10 \Omega \cdot \text{m}$; this second layer has an average thickness of 60 m. The deepest layer presents even lower resistivity values of $1\text{--}5 \Omega \cdot \text{m}$. The 4 km long profile 2, displays similar structure with the same resistivities and thicknesses.

The southern profiles have N-S (P3), WSW-ENE (P4) and NNW-SSE (P5) orientations and present much higher resistivities than the northern profiles. In P3 two layers can be differentiated: the shallower one has resistivity values higher than $1000 \Omega \cdot \text{m}$ and an average thickness of 100 m; the deeper layer presents intermediate resistivities ranging from 10 to $100 \Omega \cdot \text{m}$. The resistivity pseudo-section produced by the

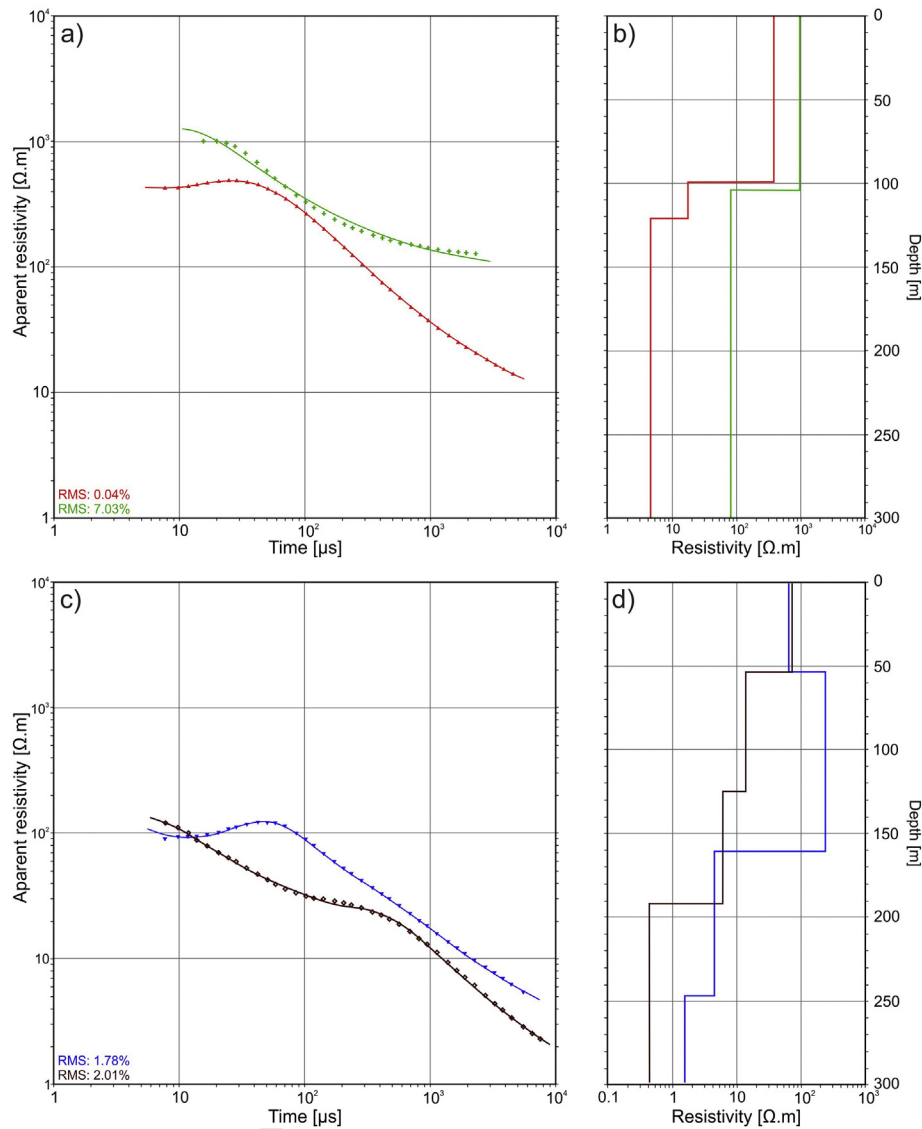


Fig. 3. TDEM curves and fitting (left) and models (right) of data from the Island of Fogo (a, b) and the Island of Santo Antão (c, d). The location of the four stations is shown in Fig. 1.

326 program – always done in horizontal layers – is not realistic due to the
 327 strong topographic contrast along the profile, and thus any interpreta-
 328 tion should be made using the values displayed beneath the soundings
 329 locations.

330 In P4 three layers can be distinguished, in which the 2 shallowest are
 331 similar to those in profile 3 although presenting different thicknesses –
 332 about 40 m for the shallower and 60 m for the intermediate layer. The
 333 deepest layer presents low resistivity values of ~5 Ω·m, especially at
 334 the E extremity. Finally, P5 presents the same 2 upper layers but the re-
 335 sistivity contrast between them are smaller than in the previous
 336 profiles.

337 5. Discussion

338 5.1. Hydrogeology of Fogo

339 There are previous studies about groundwater resources in several
 340 islands of the Cape Verde archipelago, including the N flank of Fogo Is-
 341 land (Heilweil et al., 2006). Several geophysical methods have been ap-
 342 plied on the island for water-table depth prospecting; these include
 343 vertical electrical soundings (VES) and electromagnetic resistivity profil-
 344 ing (VLF-r) along the outer flanks of the island (Kallrén and
 345 Schreiber, 1988), and TDEM surveys within the central caldera

(Descloitres et al., 2000). These investigations did not obtain successful
 346 results. 347

348 The island drainage system presents a centrifugal radial pattern com-
 349 posed of hundreds of shallow incised and weekly hierarchized water-
 350 sheds that extend from the caldera rim to the sea. The most developed
 351 watersheds are those draining the N flank of the island. The studied
 352 area covered in this research is ~270 km² on the SW side of the Island
 353 of Fogo – ranging in altitude from sea level to 2500 m a.s.l. – where 26
 354 TDEM soundings were measured.

355 The previous studies in Fogo hypothesize about groundwater distri-
 356 bution without the aid of good quality geophysical data. These studies
 357 claim that the water-table is at a relatively deep beneath the caldera
 358 (Kallrén and Schreiber, 1988; Barmen et al., 1990; Heilweil et al.,
 359 2009). The main conclusions obtained previously to our research are
 360 summarized as follows (Heilweil et al., 2012): **Q10**

- water-table is approximately at sea level as measured in five wells 361
 located at altitudes of 20–60 m a.s.l.; 362
- occurrence of abundant coastal springs (Kallrén and Schreiber, 363
 1988; Heilweil et al., 2006); 364
- water-table is present at 100 m and 180 m depths as determined 365
 from water drills located at altitudes of 300 m and 500 m a.s.l., re- 366
 spectively (Barmen et al., 1990); 367

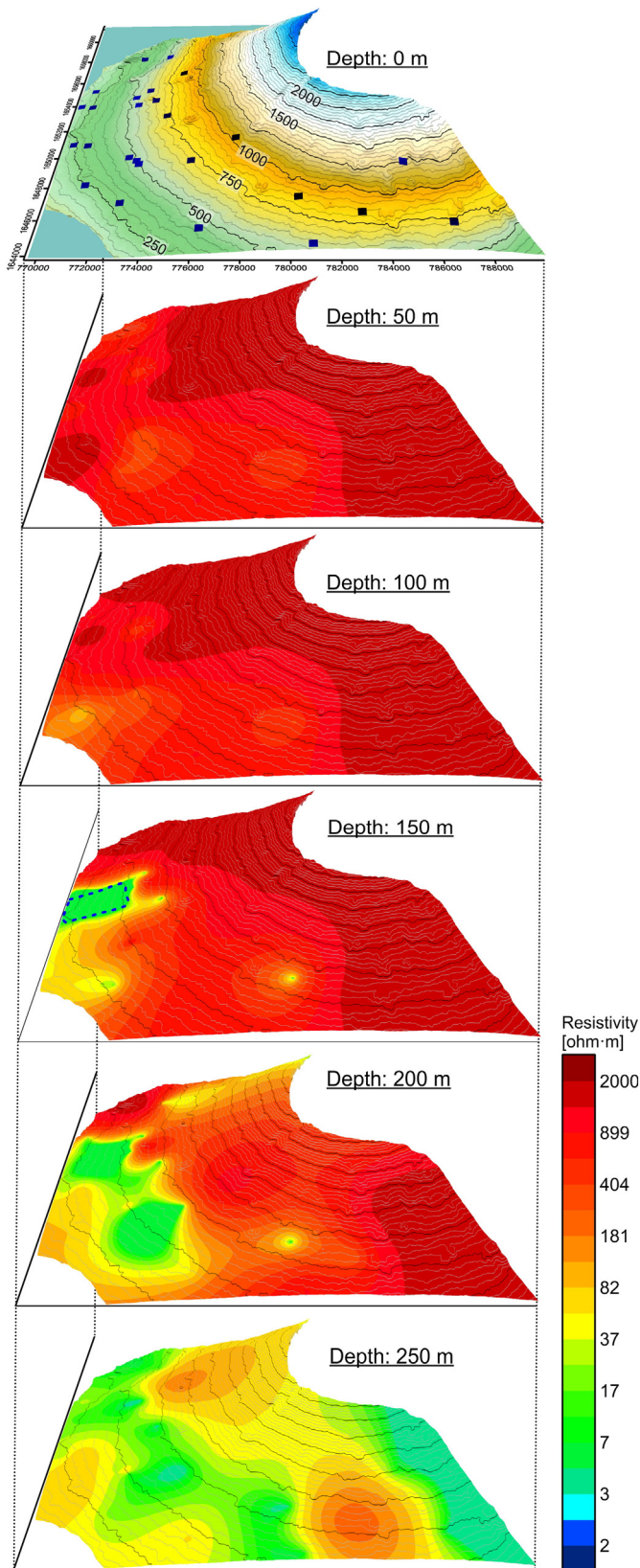


Fig. 4. 3D model of the subsurface resistivity distribution in southwest Fogo. The layers display the resistivity at every 50 m depth down to 250 m. The blue dots on the surface topographic map show the location of the TDEM stations. The blue dashed line indicates the area to be interpreted with caution due to kriging effects. (For interpretation of the references to colour in this figure legend, the reader is referred to the web version of this article.)

- water-table is deeper than 400 m beneath the caldera floor (Chã das Caldeiras) as determined from a geothermal research drill (Instituto Nacional de Gestão dos Recursos Hídricos, INGRH, 2011; <http://www.ingrh.cv>);
- TDEM surveys in Chã das Caldeiras found no evidence for the presence of water shallower than 400 m depth (Descloitres et al., 2000).

Our TDEM results indicate variable water-table depths depending on elevation (Fig. 6). High resistivities are obtained for the first 100 m below the topographical surface indicating that no water is present. Low resistivity values, indicating the presence of the water-table, appear for the first time at a depth of 150 m at elevations around 500 m a.s.l. on the west side of the study area (Fig. 4). This corresponds to the area between Monte Almada and the littoral spring of Praia Ladrão (Fig. 1b). The area with low resistivity presents a very geometrical (rectangular) shape suggesting a marked structural control – probably due to the presence of dikes – and possibly by the presence of a shallower old basement that crops out locally at Monte Almada. Low resistivities have been detected inland (up to around 750 m a.s.l.) at two soundings and to the SE at the depth of 200 m. Finally, at 250 m depth the low resistivity values extend to the whole study area up to 1000 m a.s.l. (Fig. 4). Therefore, at low topographic levels (up to 500 m a.s.l.) the water-table is located between 100 and 150 m depths, whereas in higher regions (up to 1000 m a.s.l.) the water-table is located at ~250 m depth. If we extrapolate this tendency to the island seaboard the water-table may be located at depths shallower than 100 m, while closer to the caldera rim it should be quite deep. These results are in general accordance with those obtained by Heilweil et al. (2012).

5.2. Hydrogeology of Santo Antão

Unlike the Island of Fogo, in Santo Antão there are no previous geophysical studies for water prospection, and just a few previous hydrology researches related to groundwater (Haagsma, 1995; Langworthy and Finan, 1997). For this study we measured 5 TDEM profiles corresponding to a total of 32 soundings. They cover the NE side of the island, with two profiles (P1 and P2) on the N flank and three profiles (P3–P5) in the S flank.

Remarkable differences in the resistivity values were found between the two flanks (Fig. 5). In the N profiles the average resistivity values for the unsaturated area is ~100 Ω·m, while in the S profiles resistivities are higher than 1000 Ω·m. Thus, there is a strong resistivity contrast with the northern profiles presenting resistivity values associated to the unsaturated area 10 times lower than the southern ones. Moreover, in the southern profiles P3 to P5 the water-table is deeper (~100 m) than in P1–P2 (~50–70 m).

In addition, the analysis of orthophoto image (Fig. 1c) shows marked humidity differences between the two flanks separated by the central mountain range that acts as the main water-divide of the island. These humidity differences can be highlighted comparing the dark brown shades for the N flank in contrast to the light brown ones representing the S flank; this is also expressed by the denser and more incised drainage of the slopes to the N of the central mountain range.

These contrasts in the humidity N–S conditions are explained by the action of the trade wind affecting the Cape Verde Islands (Chiapello et al., 1995). The condensation of the humidity transported by these winds, which blow almost continuously from the NE, corresponds to 1.5 to 3 times the amount of rainfall. The water vapour transported by the trade winds is condensed as the air masses climb the topographical barrier and are captured by the forest (Santamarta and Seijas, 2010). Therefore, the NE flank of the island receives most of the precipitation and the air masses that transpose the mountain range arrive to the S flank almost totally dry.

Furthermore, the northern profiles 1 and 2 (Fig. 5) show very low resistivity values, of ~1 Ω·m or lower on average, at depths of 130–100 m

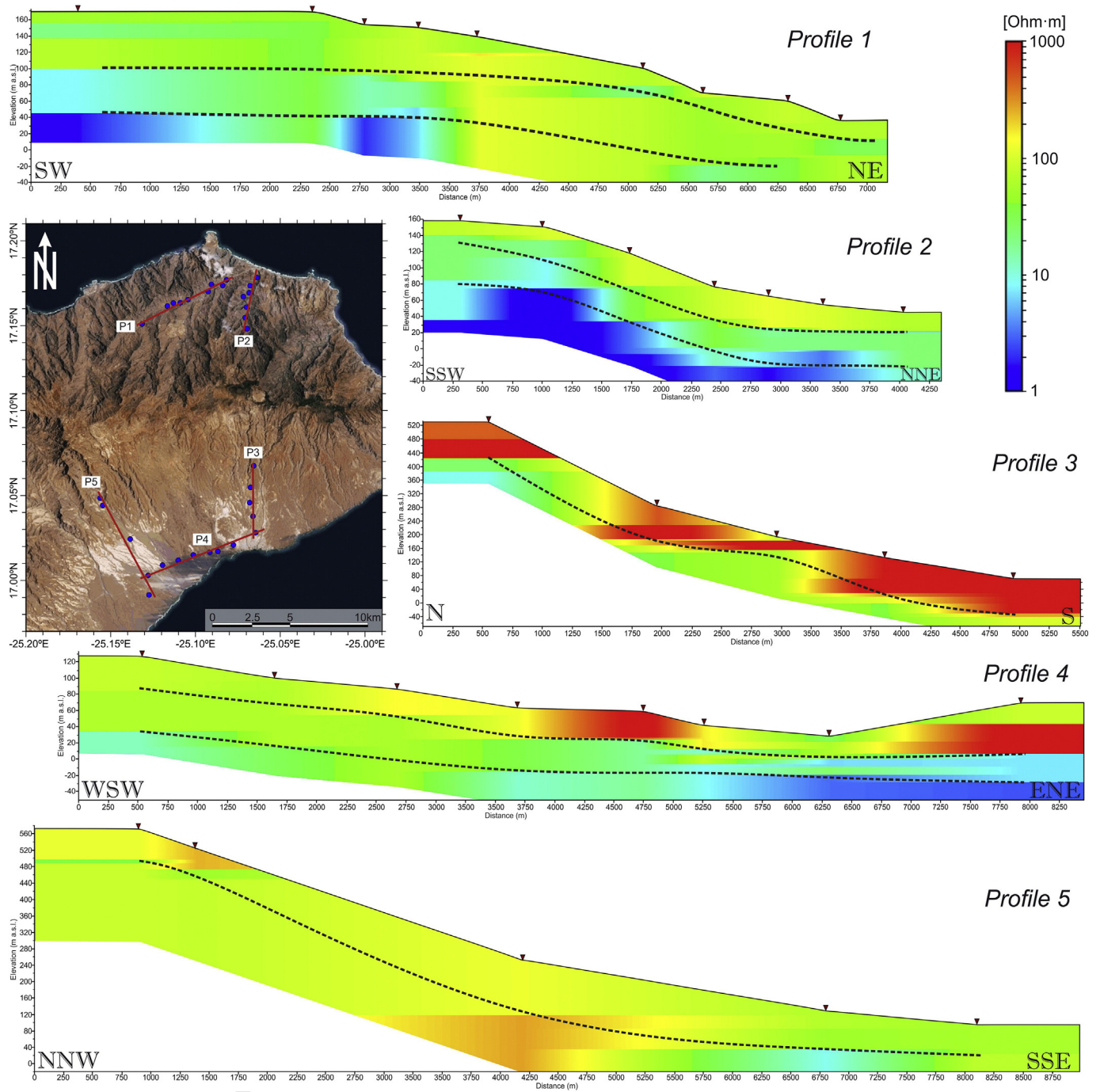


Fig. 5. Resistivity profiles and respective location in northeast Santo Antão. The blue dots on the orthophoto show the location of the TDEM stations and the red lines identify profiles P1 to P5. The dashed top lines indicate the water-table location and the bottom ones mark the fresh-water-saltwater interface. (For interpretation of the references to colour in this figure legend, the reader is referred to the web version of this article.)

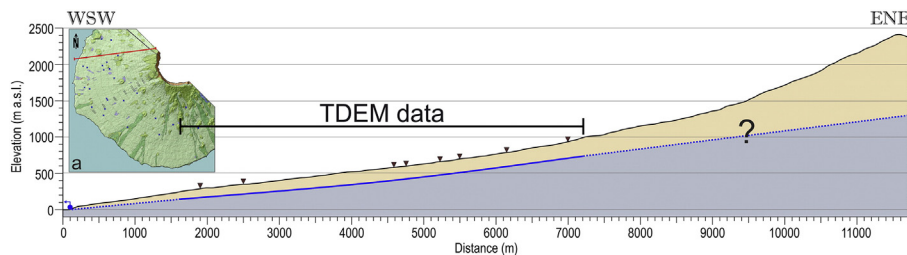


Fig. 6. Interpretative model of the water-table surface in southwest Fogo. The profile location is marked with a red line on the geological map. (For interpretation of the references to colour in this figure legend, the reader is referred to the web version of this article.)

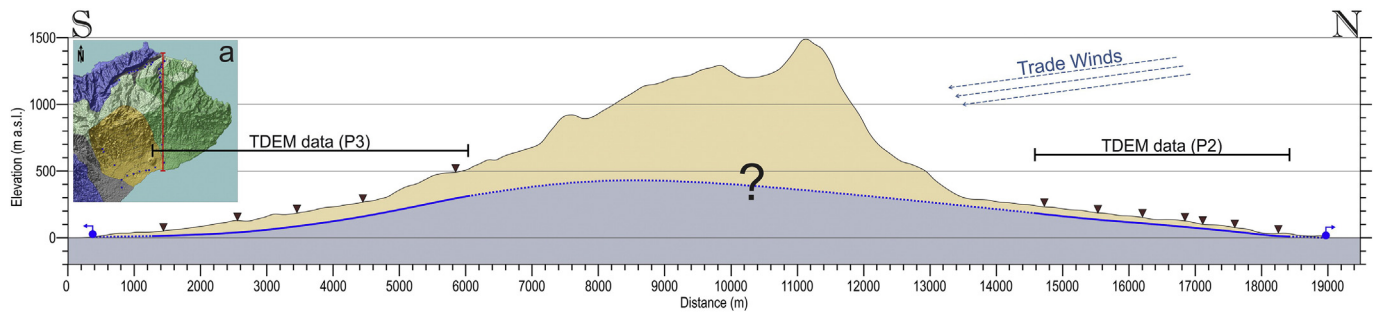


Fig. 7. Interpretative model of the water-table surface in northeast Santo Antão. The profile location is marked with a red line on the geological map. (For interpretation of the references to colour in this figure legend, the reader is referred to the web version of this article.)

431 indicating salt water intrusion. These intrusions reach altitudes of 40 m
 432 a.s.l. in P1 and around 80 m a.s.l. in P2 at the extremities further away
 433 from the shore line. This must be related with the fact that the valley
 434 bottoms of Ribeira Grande and Ribeira da Torre present a thick and
 435 highly permeable alluvial infill, with the volcanic basement below sea-
 436 level in the terminal part of their profile. This information was obtained
 437 from the owners of wells in the terminal few km of Ribeira Grande,
 438 which mentioned that the wells crossed thicknesses of gravel and
 439 sand exceeding the elevation of the site. Thus, the salt water intrusions
 440 in these areas must be taken into account when managing groundwater
 441 exploitation.

442 TDEM data obtained in both flanks of the island were used to obtain
 443 a hydrogeologic model of the water-table distribution in Santo Antão
 444 (Fig. 7). For this purpose, the data obtained in profiles 2 (N) and 3
 445 (S) were used (Fig. 5). This model shows the differences in water-
 446 table depth in the two flanks; in the southern slope the water-table is
 447 deeper (~100 m depth) than in the northern slope (~50 m depth) due
 448 to the large differences in precipitation supplied by the trade winds. In
 449 addition, we interpolated the expected water-table morphology for the
 450 central part of the island, beneath the higher ranges of the volcanic
 451 edifice, which must be located at depths in excess of 1000 m.

452 The models of Figs. 6 and 7 must be taken as approximations to the
 453 water-table morphology, since our data does not allow depicting the ef-
 454 fects of dikes swarms in the geometry of the main aquifer (Barmen et al.,
 455 1990). TDEM data allows obtaining a general model but the details of
 456 the aquifer compartments must be addressed in combination with addi-
 457 tional geological and geophysical methods.

458 6. Conclusions

459 This study used TDEM data to provide new information on ground-
 460 water distribution in the islands of Fogo and Santo Antão (Cape Verde
 461 archipelago) where previous geophysical data was scarce. In Fogo a
 462 rough 3D resistivity distribution was obtained. It consists of a distribu-
 463 tion of resistivity values covering the SW region of the island represent-
 464 ed by successive layers below the surface at 50 m depth intervals, down
 465 to a depth of 250 m. The presence of a water-table was detected at a
 466 depth of 150 m close to the western coastal areas (up to elevations of
 467 250 m a.s.l.), and at depths of 200–250 m for the whole study area up
 468 to altitudes of 1000 m a.s.l. The geometry of the water-table surface
 469 shows a shallower depth in littoral areas gradually increasing in depth
 470 up the slope.

471 TDEM data for Santo Antão was acquired along profiles located on
 472 the northern and southern slopes of the NE half of the island; the distri-
 473 bution was chosen in order to reflect the marked climatic differences
 474 between the wetter northern flank that directly receives the NE blowing
 475 dominant trade winds and the dryer southern flank. These differences
 476 are expressed in the resistivity values obtained by the TDEM profiles.
 477 In the N slope the water-table is shallower than in the S. Additionally
 478 the data allowed detecting important salt water intrusion in the N
 479 flank profiles, as well as estimating the expected geometry of the

main aquifer surface across the island, interpreted to be located at great-
 480 er depths beneath the higher reaches of the volcanic edifice. 481

482 This study demonstrates the usefulness of TDEM methods for
 483 groundwater prospecting, using both profile and areal station geomet-
 484 ries. Our results provided an approximate initial groundwater model
 485 distribution in the islands of Fogo and Santo Antão in the Republic of
 486 Cape Verde. However this is only an approximation that must be
 487 complemented with more detailed geological and geophysical studies. 488

488 Acknowledgements

489 The authors thank GESTO Energy Consulting for permission to use
 490 the data. In addition, we are grateful with the positive comments and
 491 suggestions made by two anonymous reviewers. This publication is
 492 supported by project FCT UID/GEO/50019/2013 – Instituto Dom Luiz. 492

493 References

- Ancochea, E., Huertas, M.J., Hernán, F., Brändle, J.L., 2010. Volcanic evolution of São
 494 Vicente, Cape Verde Islands: the Praia Grande landslide. *J. Volcanol. Geotherm. Res.*
 495 198, 143–157.
 Ancochea, E., Huertas, M.J., Hernán, F., Brändle, J.L., 2014. A new felsic cone-sheet swarm
 497 in the Central Atlantic Islands: the cone-sheet swarm of Boa Vista (Cape Verde).
 498 *J. Volcanol. Geotherm. Res.* 274, 1–15.
 Ancochea, E., Huertas, M.J., Hernán, F., Brändle, J.L., Alonso, M., 2015. Structure, composi-
 500 tion and age of the small islands of Santa Luzia, Branco and Raso (Cape Verde Archi-
 501 pelago). *J. Volcanol. Geotherm. Res.* 302, 257–272.
 Barmen, G., Carvalho, V., Querido, A., 1990. Groundwater-related geological and isotopic
 503 investigations on the Island of Fogo: an overview. Report LUTVDG/TVTG-90/3027.
 504 Lund University Institute of Technology, Lund, Sweden (72 pp).
 Bortolozzo, C.A., Porsani, J.L., Santos, F.A.M.d., Almeida, E.R., 2015. VES/TEM 1D joint inver-
 506 sion by using Controlled Random Search (CRS) algorithm. *J. Appl. Geophys.* 112,
 507 157–174.
 Brum da Silveira, A., Madeira, J., Serralheiro, A., 1997. A estrutura da ilha do Fogo, Cabo
 509 Verde. A erupção vulcânica de 1995 na ilha do Fogo, Cabo Verde. Instituto de
 510 Investigação Científica Tropical e Ministério da Ciência e Tecnologia, pp. 63–78.
 511 Chiappello, I., Bergametti, G., Gomes, L., Chatenet, B., Dulac, F., Pimenta, J., Santos Soares, E.,
 512 1995. An additional low layer transport of Sahelian and Saharan dust over the north-
 513 eastern tropical Atlantic. *Geophys. Res. Lett.* 22, 3191–3194.
 514 Custodio, E., 1978. *Geohidrología de terrenos e islas volcánicas*. Centro de estudios
 515 Hidrográficos, Madrid.
 Day, S.J., Heleno da Silva, S.I.N., Fonseca, J.F.B.D., 1999. A past giant lateral collapse and
 517 present-day flank instability of Fogo, Cape Verde Islands. *J. Volcanol. Geotherm. Res.*
 518 94, 191–218.
 519 Descloitres, M., Guérin, R., Albouy, Y., Tabbagh, A., Ritz, M., 2000. Improvement in TDEM
 520 sounding interpretation in presence of induced polarization. A case study in resistive
 521 rocks of the Fogo volcano, Cape Verde Islands. *J. Appl. Geophys.* 45, 1–18.
 522 Descloitres, M., Chalikakis, K., Legchenko, A., Moussa, A.M., Genthon, P., Favreau, G., Le
 523 Coz, M., Boucher, M., Oï, M., 2013. Investigation of groundwater resources in the
 524 Komadugu Yobe Valley (Lake Chad Basin, Niger) using MRS and TDEM methods.
 525 *J. Afr. Earth Sci.* 87, 71–85.
 526 Duprat, H.I., Friis, J., Holm, P.M., Grandvuinet, T., Sørensen, R.V., 2007. The volcanic and
 527 geochemical development of São Nicolau, Cape Verde Islands: constraints from
 528 field and $^{40}\text{Ar}/^{39}\text{Ar}$ evidence. *J. Volcanol. Geotherm. Res.* 162, 1–19.
 529 Dyhr, C.T., Holm, P.M., 2010. A volcanological and geochemical investigation of Boa Vista,
 530 Cape Verde Islands; $^{40}\text{Ar}/^{39}\text{Ar}$ geochronology and field constraints. *J. Volcanol.*
 531 *Geotherm. Res.* 189, 19–32.
 532 Eisele, S., Freundt, A., Kutterolf, S., Ramalho, R.S., Kwasnitschka, T., Wang, K.L., Hemming,
 533 S.R., 2015. Stratigraphy of the Pleistocene, phonolitic Cão Grande Formation on Santo
 534 Antão, Cape Verde. *J. Volcanol. Geotherm. Res.* 301, 204–220.
 535

- 536 Everett, M.E., 2013. Near-surface Applied Geophysics. Cambridge University Press, UK 415
537 pp.
- 538 Fainberg, E., 1999. TEM-Fast 48 Manual. Applied Electromagnetic Research, Amsterdam,
539 The Netherlands.
- 540 Figueira, C., de Sequeira, M.M., Vasconcelos, R., Prada, S., 2013. Cloud water interception in
541 the temperate laurel forest of Madeira Island. *Hydrol. Sci. J.* 58, 152–161.
- 542 Flint, A.L., Flint, L.E., Hevesi, J.A., Blainey, J.B., 2013. Fundamental concepts of recharge in
543 the desert southwest: a regional modeling perspective. In: Hogan, J.F., Phillips, F.M.,
544 Scanlon, B.R. (Eds.), *Groundwater Recharge in a Desert Environment: The Southwest-*
545 *ern United States*. American Geophysical Union, pp. 159–184.
- 546 Gingerich, S.B., Oki, D.S., 2000. *Ground Water in Hawaii*. U.S. Geological Survey, Fact Sheet
547 126-00 6 pp.
- 548 Goldman, M., Rabinovich, B., Rabinovich, M., Gilad, D., Gev, I., Schirov, M., 1994. Geophys-
549 ics and environment application of the integrated NMR-TDEM method in groundwa-
550 ter exploration in Israel. *J. Appl. Geophys.* 31, 27–52.
- 551 Haagsma, B., 1995. Traditional water management and state intervention: the case of
552 Santo Antão, Cape Verde. *Mt. Res. Dev.* 15, 39–56.
- 553 Heilweil, V.M., Earle, J.D., Cederberg, J.R., Messer, M.M., Jorgensen, B.E., Verstraeten, I.M.,
554 Moura, M.A., Querido, A., Spencer, S., Osorio, T., 2006. Evaluation of Baseline
555 Ground-water Conditions in the Mosteiros, Ribeira Paul, and Ribeira Fajã Basins, Re-
556 public of Cape Verde, West Africa, 2005–06. US Department of the Interior, US Geol-
557 ogical Survey.
- 558 Heilweil, V.M., Solomon, D.K., Gingerich, S.B., Verstraeten, I.M., 2009. Oxygen, hydrogen,
559 and helium isotopes for investigating groundwater systems of the Cape Verde
560 Islands, West Africa. *Hydrogeol. J.* 17, 1157–1174.
- 561 Heilweil, V.M., Healy, R.W., Harris, R.N., 2012. Noble gases and coupled heat/fluid flow
562 modeling for evaluating hydrogeologic conditions of volcanic island aquifers.
563 *J. Hydrol.* 464–465, 309–327.
- 564 Hoareau, J., Vouillamoz, J.M., Beck, M., Reddy, M., Desclotres, M., Legchenko, A., Sekhar,
565 M., Kumar, M.M., Braun, J.-J., 2007. Joint use of geophysical and hydrological methods
566 to characterize structures and flow geometry in a complex aquifer. Near Surface
567 2007–13th EAGE European Meeting of Environmental and Engineering Geophysics.
- 568 Hoernle, K., Tilton, G., Le Bas, M.J., Duggan, S., Garbe-Schönberg, D., 2002. Geochemistry of
569 oceanic carbonatites compared with continental carbonatites: mantle recycling of
570 oceanic crustal carbonate. *Contrib. Mineral. Petrol.* 142, 520–542.
- 571 Holm, P.M., Wilson, J.R., Christensen, B.P., Hansen, L., Hansen, S.L., Hein, K.M., Mortensen,
572 A.K., Pedersen, R., Plesner, S., Runge, M.K., 2006. Sampling the Cape Verde mantle
573 plume: evolution of melt compositions on Santo Antão, Cape Verde Islands.
574 *J. Petrol.* 47, 145–189.
- 575 Holm, P.M., Grandvuinet, T., Friis, J., Wilson, J.R., Barker, A.K., Plesner, S., 2008. An
576 ^{40}Ar – ^{39}Ar study of the Cape Verde hot spot: temporal evolution in a semistationary
577 plate environment. *J. Geophys. Res. Solid Earth* 113.
- 578 Jackson, D.B., Lenat, J.F., 1989. High-level Water Tables on Hawaiian Type Volcanoes and
579 Intermediate Depth Geoelectric Structures, Kilauea Volcano, Hawaii and Piton de la
580 Fournaise Volcano, Isle de la Reunion. New Mexico Bureau of Geology & Mineral Re-
581 sources, pp. 131–142.
- 582 Johnson, M.E., Ramalho, R.S., Baarli, B.G., Cachão, M., da Silva, C.M., Mayoral, E.J., Santos, A.,
583 2014. Miocene–Pliocene rocky shores on São Nicolau (Cape Verde Islands): contrast-
584 ing windward and leeward biofacies on a volcanically active oceanic island.
585 *Palaeogeogr. Palaeoclimatol. Palaeoecol.* 395, 131–143.
- 586 Kallrén, L., Schreiber, I., 1988. Groundwater survey on western Fogo, Cape Verde. Report
587 TVTG-5019. Lund Institute of Technology, Lund, Sweden.
- 588 Langworthy, M., Finan, T.J., 1997. *Waiting for Rain: Agriculture and Ecological Imbalance*
589 *in Cape Verde*. Lynne Rienner Publishers.
- 590 Liu, C.C., Lau, L.S., Mink, J.F., 1983. Ground water model for a thick fresh water lens.
591 *Ground Water* 21, 293–300.
- 592 López-Guzmán, T., Alector Ribeiro, M., Orgaz-Agüera, F., Marmolejo Martín, J.A., 2015. El
593 turismo en Cabo Verde: Perfil y valoración del viajero. *Estud. Perspect. Tur.* 24,
594 512–528.
- 595 Macdonald, G.A., Abbott, A.T., Peterson, F.L., 1983. *Volcanoes in the Sea: The Geology of*
596 *Hawaii*. 2nd edn. University of Hawaii Press, Honolulu.
- 597 Madeira, J., Brum da Silveira, A., Mata, J., Mourão, C., Martins, S., 2008. The role of mass
598 movements on the geomorphologic evolution of island volcanoes: examples from
599 Fogo and Brava in the Cape Verde archipelago. *Comun. Geol.* 95, 93–106.
- 600 Madeira, J., Mata, J., Mourão, C., da Silveira, A.B., Martins, S., Ramalho, R., Hoffmann, D.L.,
601 2010. Volcano-stratigraphic and structural evolution of Brava Island (Cape Verde)
602 based on $^{40}\text{Ar}/^{39}\text{Ar}$, U–Th and field constraints. *J. Volcanol. Geotherm. Res.* 196,
603 219–235.
- 604 Marques, R., Prudêncio, M.I., Waerenborgh, J.C., Rocha, F., Dias, M.I., Ruiz, F., Ferreira da
605 Silva, E., Abad, M., Muñoz, A.M., 2014. Origin of reddening in a paleosol buried by
606 lava flows in Fogo island (Cape Verde). *J. Afr. Earth Sci.* 96, 60–70.
- 607 Martí, J., Hurlimann, M., Ablay, G.J., Gudmundsson, A., 1997. Vertical and lateral collapses
608 on Tenerife (Canary Islands) and other volcanic ocean islands. *Geology* 25, 879–882.
- 609 Mitchell, J.G., Le Bas, M.J., Zielonka, J., Furnes, H., 1983. On dating the magmatism of Maio,
610 Cape Verde Islands. *Earth Planet. Sci. Lett.* 64, 61–76.
- 611 Nabighian, M.N., 1988. *Electromagnetic Methods in Applied Geophysics*. SEG Books.
- 612 Nicaise, Y., Marc, D., Michel, V.J., Christian, A., 2013. Delimitation of the salt water wedge
613 in the shallow coastal aquifer by TDEM method at Togbin (South Benin). *Int. J. Adv.*
614 *Sci. Technol.*
- 615 Plesner, S., Holm, P.M., Wilson, J.R., 2003. ^{40}Ar – ^{39}Ar geochronology of Santo Antão, Cape
616 Verde Islands. *J. Volcanol. Geotherm. Res.* 120, 103–121.
- 617 Ramalho, R., Helffrich, G., Schmidt, D., Vance, D., 2010. Tracers of uplift and subsidence in
618 the Cape Verde archipelago. *J. Geol. Soc.* 167, 519–538.
- 619 Ramalho, R.S., Winckler, G., Madeira, J., Helffrich, G.R., Hipólito, A., Quartau, R., Adena, K.,
620 Schaefer, J.M., 2015. Hazard potential of volcanic flank collapses raised by new
621 megatsunami evidence. *Sci. Adv.* 1, e1500456.
- 622 Ribeiro, O., 1960. *A Ilha do Fogo e as suas Erupções-Memórias*. (Série geográfica 1). Junta
623 de Investigação do Ultramar. 2nd Ed. Lisboa, Portugal. 319 pp. In Portuguese, Lisboa
624 (Portugal).
- 625 Ruiz-Constán, A., Pedreira, A., Martos-Rosillo, S., Galindo-Zaldívar, J., Martín-Montañés, C.,
626 González De Aguilar, J.P., 2015. Structure of a complex carbonate aquifer by magnetic,
627 gravity and TDEM prospecting in the JAÉN area, Southern Spain. *Geol. Acta* 13,
628 191–203.
- 629 Sananikone, K., 1998. Subsurface Characterization Using Time-domain Electromagnetics
630 at the Texas a&M University Brazos River Hydrologic Field Site, Burleson County,
631 Texas. Texas A&M University.
- 632 Santamarta Cerezal, J.C., 2013. *Hidrología y recursos hídricos en islas y terrenos*
633 *volcánicos*. Colegio de Ingenieros de Montes, Tenerife.
- 634 Santamarta Cerezal, J.C., Seijas Bayón, J., 2010. Fundamentos y tecnologías para la
635 captación y uso del agua procedente de la lluvia horizontal en los montes canarios.
636 *Montes: revista de ámbito forestal* 100, pp. 15–21.
- 637 Torres, P.C., Madeira, J., Silva, L.C., Brum da Silveira, A., Serralheiro, A., Mota Gomes, A.,
638 1998. Carta geológica da Ilha do Fogo (República de Cabo Verde): erupções históricas
639 e formações enquadantes. Geological Map. Ed. Lattex, 1 Sheet at 1:25.000 Scale.
- 640 Torres, P., Silva, L., Serralheiro, A., Tassinari, C., Munhá, J., 2002. Enquadramento
641 geocronológico pelo método K/Ar das principais sequências vulcano-estratigráficas
642 da Ilha do Sal–Cabo Verde. *García de Orta, Série Geológica* 18, pp. 9–13.
- 643 Ward, S.H., Hoekstra, P., Blohm, M.W., 1990. 1. Case histories of time-domain electromag-
644 netic soundings in environmental geophysics. *Geotechnical and Environmental Geo-*
645 *physics*. Society of Exploration Geophysicists, pp. 1–16.
- 646 White, R.S., 1989. Asthenospheric control on magmatism in the ocean basins. *Geol. Soc.*
647 *Lond., Spec. Publ.* 42, 17–27.
- 648 Yechieli, Y., Kafri, U., Goldman, M., Voss, C., 2001. Factors controlling the configuration of
649 the fresh–saline water interface in the Dead Sea coastal aquifers: synthesis of TDEM
650 surveys and numerical groundwater modeling. *Hydrogeol. J.* 9, 367–377.